Results in Physics 68 (2025) 108093

Contents lists available at ScienceDirect

Results in Physics

journal homepage: www.elsevier.com/locate/rinp

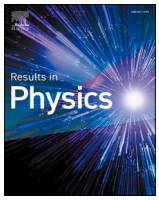

Influence of coulomb effects on electron dynamics in orthogonally polarized two-color laser fields

Hristina S. Delibašić-Marković [a,*], Violeta M. Petrović [a], Ivan D. Petrović [b]

[a] University of Kragujevac, Faculty of Science, Radoja Domanovića 12, 34000 Kragujevac, Serbia
[b] Academy of Professional Studies Šumadija, Department in Kragujevac, Kosovska 8, 34000 Kragujevac, Serbia

ARTICLE INFO

Keywords:
Tunneling ionization
OTC field
Ionization rate
Coulomb

ABSTRACT

This study examines the ionization dynamics of argon atoms under orthogonally polarized two-color laser fields, highlighting the impact of field strength ratio on ionization rates and electron momentum. Utilizing a theoretical framework, we compare our results with various models to delineate the effects of Coulomb potential across different field strength ratios. The investigation reveals that the distribution of electric field strength over orthogonal components influences the ionization efficiency, with variations in ionization rates and momentum distributions across a range of intensities. Our findings contribute to a deeper understanding of strong-field ionization processes, providing insights into the interplay between field geometry and electron dynamics.

Introduction

Tunneling ionization (TI), driven by intense laser fields, stands as a cornerstone process in atomic, molecular, and optical physics, facilitating cutting-edge developments in applications such as control of chemical reactions [1], manipulation of quantum states [2], attosecond pulse generation [3], spectroscopy of highly excited states [4], and the nuanced characterization of acoustic metamaterials [5]. This mechanism involves an electromagnetic field altering the Coulomb potential, allowing a bound electron to tunnel through a newly-formed barrier, which significantly influences electron dynamics at the tunnel exit, especially under different laser field polarizations [6,7]. Studies in this field have deepened our understanding of interactions within high-intensity fields, showing important implications for both theoretical and experimental physics [8]. The field explores a variety of phenomena that occur when driven electrons interact with their atomic or molecular cores. These phenomena include above-threshold ionization (ATI) [9], nonsequential double ionization (NSDI) [10], high-order harmonic generation (HHG) [11], spin polarization [12], photoelectron holography [13], electron diffraction patterns [14], dynamics of electron recollision [15], laser-induced filamentation [16], and the creation of laser-produced plasma (LIP) channels [17]. The insights gained from studying these interactions have improved theoretical models and experimental methods, furthering the field of strong-field physics.

Building on the foundational understanding of TI, semiclassical approaches such as those developed by Keldysh [18], Perelomov, Popov, and Terentiev (PPT) [19], as well as Ammosov, Delone and Krainov (ADK) [20], deepened our understanding of electron behavior in intense laser fields. The Keldysh model [18], often referred to as 'optical tunneling,' effectively categorized the ionization process into TI and multiphoton ionization (MPI). It uses the dimensionless parameter γ, where $\gamma \ll 1$ indicates tunneling through a laser-modified Coulomb barrier, and $\gamma \gg 1$ points to MPI, involving electrons absorbing multiple photons to escape the atomic potential. The introduction of the PPT theory [19] marked a significant enhancement of the Keldysh model by incorporating the effects of the Coulomb potential more accurately, thus enabling a more nuanced understanding of electron dynamics both during and after the tunneling process. This refinement was crucial in linking quantum mechanical and classical descriptions of ionization, enhancing the theoretical framework for analyzing electron interactions under extreme field conditions. Building on these semiclassical models, the Strong Field Approximation (SFA) [21] simplified the interaction dynamics by focusing primarily on the electron and the laser field. This approximation was crucial for developing detailed insights into ionization processes, especially in scenarios where the Coulomb potential's influence was minimal, such as in certain high-intensity laser interactions. Furthermore, the ADK model [20] refined the TI approach by employing a quasi-static approximation, considering the changes in the laser field to be gradual compared to the response of the atomic system. This helped to understand how slow variations in the laser field affected

* Corresponding author.
E-mail address: hristina.delibasic@pmf.kg.ac.rs (H.S. Delibašić-Marković).

https://doi.org/10.1016/j.rinp.2024.108093
Received 15 July 2024; Received in revised form 6 December 2024; Accepted 15 December 2024
Available online 16 December 2024

ionization dynamics. Beyond these semiclassical approximations, the time-dependent Schrödinger equation (TDSE) [22] provided a full quantum mechanical description of the interaction between an atom and an intense laser field. Solving the TDSE enabled precise predictions of electron dynamics, capturing the complete spectrum of laser-induced phenomena without the simplifications presented in models like ADK [20] or SFA [21]. This approach was particularly important in scenarios where the laser's temporal evolution significantly influenced electron motion, providing a comprehensive microscopic understanding of the process. Additional theoretical contributions by Faisal [23] and Reiss [24] have further enriched this field. They introduced the Faisal-Reiss theory [25], which, like SFA [21], focuses on the interaction between the electron and the laser field. However, this theory integrates the Coulomb potential more effectively, better accounting for its effects in strong field environments. Reiss's work (see [24]) has provided deep insights into the roles of both the laser and Coulomb fields in shaping electron trajectories during ionization. Moreover, a study by Becker et al. [26] revisited the influence of the Coulomb potential on the ionization process, offering critical insights that have sparked renewed interest and deeper investigations into Coulomb effects. Becker's study [26], in particular, highlighted how Coulomb forces can alter predicted ionization rates and electron trajectories, challenging some of the assumptions made in earlier models (see [27] for details).

Recent advancements in strong-field physics have increasingly focused on the significant role of elliptical polarization in TI and its interplay with Coulomb forces [28–30]. This interest is driven by the need to better understand and manipulate electron dynamics under various polarization conditions, which directly affect ionization outcomes and electron trajectory behaviors. Both experimental and theoretical research has deepened our understanding of these dynamics. For instance, a study by Huang et al. [31] utilized near-circularly polarized laser fields to examine electron momentum distributions in argon (*Ar*), revealing an unexpected narrowing of transverse momentum distributions with increasing laser intensity – a phenomenon attributed to Coulomb focusing due to temporary trapping by the atomic potential. This observation challenges the conventional views held by adiabatic theories and underscores the critical role of elliptical polarization in electron dynamics. Additionally, Zhao's group [32] studied frustrated tunneling ionization (FTI) in elliptically polarized fields, discovering that ionization yields peak at specific ellipticities. This finding suggests that the initial conditions of electron ejection, especially the transverse velocity, are closely tied to the laser's polarization characteristics. Further, Geyer et al. [33] provided crucial experimental data showing variability in the initial momentum component of electrons in *Ar* atoms, which shifts in response to the dynamic changes in the field. This behavior enhances the Coulomb interaction between the outgoing electron and its parent ion, highlighting the importance of elliptical polarization in shaping ionization dynamics. On the theoretical side, Zhang and colleagues [34] employed the SFA and saddle point methods to numerically explore the Coulomb effect on bouquet-like photoelectron momentum distributions. Their work showed significant changes in low momentum ranges, enhancing our understanding of how Coulomb forces influence interference patterns in these distributions. Additionally, Feng et al. [35] analyzed photoelectron interferometry in ATI regimes using synthesized two-color laser pulses. Their work provided new insights into the phase-dependent behavior of photoelectron energy spectra, offering a method to more precisely control photoelectron outcomes. The collective contributions from these studies [28–35] are profoundly shaping the fields of strong-field and attosecond physics. As research continues to explore the effects of field strength ratio and Coulomb interactions, it promises to unlock new technological applications in areas such as precision spectroscopy [35] and the exploration of ultrafast electron dynamics [36].

In the domain of strong-field physics, the present study employs orthogonally polarized two-color (OTC) laser fields to investigate the interactions between intense laser fields and *Ar* atoms. This setup merges two laser beams with orthogonal polarizations, enabling precise control over electron ionization by adjusting the field strength ratio and exploring the impact of different polarization geometries on electron dynamics. These changes affect the intensity and orientation of electric fields interacting with atomic electrons, significantly influencing ionization pathways and the energy states accessed during these interactions. Our study builds on the foundational work of Xie et al. [37], who identified deviations in ionization timing from the peak of the laser field within OTC configurations. Their research revealed that peak tunneling rates do not necessarily coincide with the peak electric field, challenging traditional assumptions that equate peak field strength with the shortest tunneling barrier. They demonstrated how shifts in initial momentum at the tunnel exit can lead to significant variations in ionization timing, which depends on the level of nonadiabaticity in the electron tunneling process. Expanding upon these insights, our research explores the impact of Coulomb corrections on both the instantaneous ionization rate and the electron's final momentum. This aspect offers new perspectives on how the Coulomb potential influences ionization dynamics. In this study, we adjust the field strength ratio to explore how different laser field configurations influence electron dynamics. This adjustment impacts the electric field's intensity and orientation, significantly affecting ionization trajectories and the accessible energy states for electrons. By exploring these variations, we gain insights into how changes in field strength reshape the potential barriers electrons must tunnel through. Previous research shows that the shape and stability of these barriers are crucial for determining when and how electrons escape from atoms. Fields with a dominant component cause rapid changes in barrier shape, closely following the peaks and troughs of the electric field [28,31]. In contrast, fields with balanced components tend to maintain a more constant barrier, allowing for a steadier release of electrons [32]. Understanding these effects is essential for accurately assessing ionization rates and the energy of ejected electrons, which are critical for developing technologies like attosecond pulse generation [3]. Our study enhances existing models by incorporating Coulomb corrections, aiming to improve our predictions of how electrons react to various field conditions. This approach, inspired by the work of Xie et al. [37], gives us a deeper understanding of electron behavior, especially when they encounter rapid changes that challenge the traditional models. By refining the SFA models [31,34,38], our research not only advances theoretical predictions but also supports the design of better experiments in the field of strong-field physics.

The remainder of this paper is structured to systematically outline our findings and analyses. Section II explores the theoretical framework of our study. Here, we utilize the SFA method to calculate the unperturbed instantaneous ionization rates and detail the derivations of the initial and drift momenta of electrons in OTC laser fields. Additionally, incorporates the Coulomb force into our model, providing a comprehensive derivation of the resultant electron trajectories. In Section III, we present our theoretical model and compare our results with existing theoretical and experimental studies to validate our approach and discuss its broader implications. Section IV offers concluding remarks, summarizing the main insights of our research and exploring their potential impact on future studies in strong-field physics. Throughout this paper, we use atomic units to ensure consistency in our quantitative analyses, unless stated otherwise.

Theoretical framework

In the field of strong-field physics, the interaction between intense laser fields and atomic or molecular systems not only pushes the boundaries of our fundamental understanding of quantum dynamics but also paves the way for groundbreaking technological advancements [9–17,36,38]. OTC laser fields, where lasers of orthogonal polarization are superposed, provide a unique experimental setup that enables precise control over the electron dynamics during ionization, and a critical aspect for applications such as control of quantum states [39] and

ionization-based microscopy [40]. Building upon methodologies similar to those we employed in our previous work (see Ref. [28]), this study adapts our established framework to the specificities of OTC fields, highlighting the nuanced effects of laser field configuration on ionization dynamics.

Ionization dynamics in the absence of Coulomb potential

To delve deeply into ionization dynamics, it's essential to first consider scenarios that exclude the Coulomb interaction with the atomic nucleus. The approach presented in this subsection, referred to as analyzing 'unperturbed' ionization rates, isolates the electron's interaction with the laser field, while setting aside the complicated effects of the nucleus' Coulomb force. This method allows us to directly observe how various characteristics of the electric field – such as its intensity, field strength ratio, and temporal dynamics – impact the electron's liberation from its atomic bond. By doing so, we establish a foundational understanding of how the laser field alone influences ionization. This step is crucial as it provides a clear basis from which to later integrate and assess the complexities introduced by the Coulomb potential, thereby enriching our understanding of the full ionization process.

Transitioning from this fundamental analysis to more intricate scenarios, we incorporate the orthogonal polarization dynamics of OTC fields. These fields merge two laser beams with orthogonal polarizations [41], described mathematically by their electric field $\vec{E}(t)$ and vector potential $\vec{A}(t)$, given as:

$$\vec{E}(t) = E_0\left[\cos[\omega t]\,\vec{e}_x + \varepsilon \sin[2\omega t]\,\vec{e}_y\right] \tag{1}$$

$$\vec{A}(t) = -\frac{E_0}{\omega}\left[\sin[\omega t]\,\vec{e}_x - \frac{\varepsilon}{2}\cos[2\omega t]\,\vec{e}_y\right] \tag{2}$$

Here, E_0 is a laser field amplitude, ε is the ratio of the electric-field strength, while ω is the angular frequency dictating the energy of the photons. The vectors $\vec{e}_x$ and $\vec{e}_y$ serve as unit polarization vectors that establish the xy-polarization plane, essential for understanding how these fields influence electron motion and subsequently ionization dynamics (see Section 3). By adopting the dipole approximation in our analysis, we focus exclusively on the temporal aspects of the electric field, simplifying our theoretical model by assuming $\vec{E}(\vec{r}, t) \rightarrow \vec{E}(t)$ [42]. This approximation is justified as the spatial variations of the electric field are considerably less significant than the temporal effects, especially in the context of intense laser interactions with atoms where field gradients across an atom are minimal. In our approach, we account for a trapezoidal pulse envelope, $f(t)$, which features a ramp-up phase over two optical cycles, maintains a constant amplitude for six cycles, and then concludes with a ramp-down over the final two cycles. Although this envelope function is not directly shown in Eqs. (1) and (2), it is implicitly included in our analysis. We focus on the sections of the pulse where the amplitude is steady and at its maximum. This allows us to isolate and study the effects of polarization and field strength ratio more clearly during peak field conditions, which are crucial for understanding how these parameters influence ionization dynamics. By assuming the envelope is constant at its peak in our primary equations, we simplify the complex interactions for clearer analytical insights, while still grounding our model in the realistic temporal dynamics typically observed in experimental laser pulse applications.

Within the analytical construct of the SFA [21], we simplify the complex quantum mechanical interactions between the laser field and the electron to facilitate the study of electron dynamics during ionization. The SFA effectively reduces the interaction to the essential elements necessary to understand how an electron transitions from a bound state, i, to a continuum state, f, a process profoundly influenced by the configuration of the applied electric field. In this framework, the ionization rate W is computed using the saddle-point method, a powerful technique in theoretical physics that identifies the critical paths or 'quantum orbits' which contribute significantly to the semiclassical action (the action in the following), S. The action, integral to understanding the dynamics under the laser field, is expressed as:

$$W \propto \exp[-2\mathrm{Im}\{S\}] \tag{3}$$

$$S = -\int_{t_s}^{t_0} \left(E_f(t) - E_i(t)\right) dt \tag{4}$$

where, $E_i(t)$ and $E_f(t)$ are the initial and final energy states of the electron, respectively. It is important to note that the complex ionization time t_s represents a crucial parameter in the ionization process and it can be derived using the relation $t_s = t_0 + it_t$. Here, the real part, $t_0 = \mathrm{Re}\{t_s\}$, marks the physical time during the laser cycle when the electron is most likely to escape the atomic potential. It is determined by the laser field reaching an intensity sufficient to either significantly lower the potential barrier or allow the electron to absorb enough energy to overcome the barrier outright. Additionally, the term, $t_t = \mathrm{Im}\{t_s\}$, describes the duration for which the electron undergoes the quantum mechanical process of tunneling. In this context, tunneling refers to the probability of an electron passing through the barrier even if it classically lacks sufficient energy to do so. This time quantifies the extent of the barrier's influence on the electron, impacting the ionization rate exponentially. It is documented in [43] that the imaginary part of the semiclassical action, $\mathrm{Im}\{S\}$, directly correlates with the TI time and plays an important role in determining the ionization rate, W, through the relation given in Eq. (3). This relationship underscores the exponential sensitivity of ionization to the parameters governing the electron's interaction with the barrier – particularly the strength and duration of the electric field, as modulated by the laser's properties. Conversely, the real part of the action, $\mathrm{Re}\{S\}$, contributes to the phase shift experienced by the electron as it propagates under the barrier. This phase shift influences the electron's trajectory but does not directly affect the probability of ionization. This aspect of the action, while critical for understanding the full dynamics of the electron in the laser field, does not alter the probability of the electron escaping the atomic potential. This theoretical approach, supported by references to foundational studies such as those in [7,28], allows us to dissect and quantify the nuances of electron dynamics during strong-field interactions (SFI).

Building on the formulation of the action in Eq. (4), we refine our description by specifically considering the initial, $E_i(t)$, and final, $E_f(t)$, energy states of the electron during the ionization process under the influence of a laser field [44]. The initial energy state, $E_i(t)$, is quantified using the ionization potential I_p, set as $E_i(t) = -I_p$. For the final state energy $E_f(t)$, we consider the electron's kinetic energy influenced by the field, defined as $E_f(t) = \frac{1}{2}\left(\vec{p} + \vec{A}(t)\right)^2$. In this expression, $\vec{p}$ symbolizes the electron's drift momentum – conserved during its interaction with the laser field – and is represented as $\vec{p} = p_x\vec{e}_x + p_y\vec{e}_y$. Now we can reformulate the action as follows:

$$S\{\vec{p}\} = -\int_{t_s}^{t_0} \left(\frac{1}{2}\left(\vec{p} + \vec{A}(t)\right)^2 + I_p\right) dt \tag{5}$$

The action is evaluated along the most probable subbarrier trajectory, which represents the path an electron is most likely to take as it tunnels from a bound state, i, within an atom to a free state, f, influenced by the laser field. In this context, the action integral accumulates the phase the electron gains while moving under the potential barrier formed by its atomic potential and the electric field of the laser. This phase is crucial as it determines the ionization rate of the electron successfully tunneling through the barrier – a probability that exponentially depends on the imaginary part of the action.

By substituting the vector potential from Eq. (2) into Eq. (5), we can express the action as a composite of integrals:

$$S\left\{p_x, p_y\right\} = -\int_{t_s}^{t_0}\left(\frac{p_x^2+p_y^2}{2}+I_p\right)dt - \frac{1}{2}\int_{t_s}^{t_0}A_x^2 dt - \frac{1}{2}\int_{t_s}^{t_0}A_y^2 dt - \int_{t_s}^{t_0}p_x A_x dt - \int_{t_s}^{t_0}p_y A_y dt \tag{6}$$

Following the integration, the expression for the imaginary part of the action, $\mathrm{Im}\left\{S\left\{p_x, p_y\right\}\right\}$, which directly influences the ionization rate, is given by:

$$G \equiv \mathrm{Im}\left\{S\left\{p_x, p_y\right\}\right\} = \left(\frac{p_x^2+p_y^2}{2}+I_p+\frac{E_0^2}{4\omega^2}\left(1+\frac{\varepsilon^2}{4}\right)\right)t_t + \frac{E_0^2\varepsilon^2}{64\omega^3}\sinh[4\omega t_t]\cos[4\omega t_0] - \frac{E_0^2}{8\omega^3}\sinh[2\omega t_t]\cos[2\omega t_0] - p_x\frac{E_0}{\omega^2}\sin[\omega t_0]\sinh[\omega t_t] + p_y\frac{E_0}{4\omega^2}\cos[2\omega t_0]\sinh[2\omega t_t] \tag{7}$$

Within this expression, the term $\frac{E_0^2}{4\omega^2}\left(1+\frac{\varepsilon^2}{4}\right)$ presents the ponderomotive potential, U_p, in the OTC laser field. The ponderomotive potential quantifies the cycle-averaged, or quiver, energy of an electron in the oscillating electric field, integral to understanding the energetics of free electrons under laser irradiation. Physically, it acts as a confining potential that influences the motion of the electron by modulating the effective height and shape of the barrier through which the electron must tunnel to achieve ionization. In the setting of SFI, particularly with OTC fields where the field strength ratio serves as a critical parameter, the ponderomotive potential, U_p, becomes even more significant. The variation in field strength ratio introduces asymmetry in the electric field oscillations, affecting how the electron gains or loses energy during each cycle.

Refining our understanding of electron dynamics as they emerge from TI, we address the kinematic details at the exit of the potential barrier. Challenging the commonly assumed zero initial momentum of the ejected photoelectron, $\vec{v}=0$ [45], we incorporate model that consider a non-zero initial momentum [46]. This approach stems from the fundamental kinematic relation, $\vec{v} = \vec{p} + \vec{A}(t_0)$, where $\vec{p}$ represents the electron's conserved canonical momentum, and $\vec{A}(t_0)$ is the vector potential at the moment of ionization. To quantitatively analyze this, we relate the components of the conserved canonical momentum $\vec{p}\left\{p_x, p_y\right\}$ to the electron's momentum at the tunnel exit, $\vec{v}\{v\|, v_\perp\}$, through the following expressions:

$$p_x\{v\|, v_\perp\} = \alpha\{t,\omega\}(v\|\cos[\omega t_0] - v_\perp\varepsilon\sin[2\omega t_0]) + \frac{E_0}{\omega}\sin[\omega t_0] \tag{8a}$$

$$p_y\{v\|, v_\perp\} = \alpha\{t_0,\omega\}(v\|\varepsilon\sin[2\omega t_0] + v_\perp\cos[\omega t_0]) - \frac{\varepsilon E_0}{2\omega}\cos[2\omega t_0] \tag{8b}$$

Here, $\alpha\{t_0,\omega\} = 1/\sqrt{\cos^2[\omega t_0]+\varepsilon^2\sin^2[2\omega t_0]}$ is a scaling factor that adjusts the momentum components based on the laser field's polarization characteristics at the moment of ionization, t_0. It is important to note that, $v\|$ and $v_\perp$ are defined with respect to the instantaneous polarization axis of the laser field at the moment of ionization. This orientation is essential for accurately capturing how the field's strength ratio affects the electron's initial conditions at the tunnel exit, which in turn influences its subsequent trajectory and kinetic energy. This set of equations offers a detailed insight into the interaction between the laser's field configuration and the electron's initial conditions, shaping our understanding of their effects on electron dynamics.

Now, by substituting Eqs. 8 into Eq. (7), we obtain:

$$G\{v\|, v_\perp\} = \left(\frac{v_\|^2+v_\perp^2}{2}+\alpha\{t_0,\omega\}\frac{\varepsilon E_0}{\omega}\left(\frac{1}{2}\cos[\omega t_0]\cos[2\omega t_0] - \sin[\omega t_0]\sin[2\omega t_0]\right)v_\perp + \alpha\{t_0,\omega\}\frac{E_0}{\omega}\left(\cos[\omega t_0]\sin[\omega t_0] - \frac{\varepsilon^2}{2}\cos[2\omega t_0]\sin[2\omega t_0]\right)v\| + \frac{E_0^2\varepsilon^2}{8\omega^2}\cos^2[2\omega t_0] + \frac{E_0^2}{2\omega^2}\sin^2[\omega t_0] + I_p + \frac{E_0^2}{4\omega^2}\left(1+\frac{\varepsilon^2}{4}\right)\right)t_t + \frac{E_0^2\varepsilon^2}{64\omega^3}\sinh[4\omega t_t]\cos[4\omega t_0] - \frac{E_0^2}{8\omega^3}\sinh[2\omega t_t]\cos[2\omega t_0] - \alpha\{t_0,\omega\}\frac{E_0}{2\omega^2}\left(\sin[2\omega t_0]\sinh[\omega t_t] + \frac{\varepsilon}{4}\sin[4\omega t_0]\sinh[2\omega t_t]\right)v\| + \alpha\{t_0,\omega\}\frac{E_0}{\omega^2}\left(\varepsilon\sin[\omega t_0]\sin[2\omega t_0]\sinh[\omega t_t] + \frac{1}{4}\cos[\omega t_0]\cos[2\omega t_0]\sinh[2\omega t_t]\right)v_\perp - \frac{E_0^2}{\omega^3}\sin^2[\omega t_0]\sinh[\omega t_t] - \frac{\varepsilon E_0^2}{8\omega^3}\cos^2[2\omega t_0]\sinh[\omega t_t] \tag{9}$$

In exploring the dynamics of strong-field ionization, particular attention is paid to the components of electron momentum at ionization, distinguished between longitudinal $v\|$ and transversal $v_\perp$ components. While $v\|$ is linked to the ionization time t_0 as indicated by Xie et al. [37], the transversal momentum $v_\perp$ plays a vital role and is subject to specific dynamics at deriving the ionization rate expression $G\{v\|, v_\perp\}$. To determine the most probable value of $v_\perp$ at ionization, we start by setting the condition: $\partial S\{v\|, v_\perp\}/\partial v_\perp = 0$. This derivative leads to a critical balance equation that must be satisfied at the point of ionization:

$$\left(v_\perp + \alpha\{t_0,\omega\}\frac{\varepsilon E_0}{\omega}\left(\frac{1}{2}\cos[\omega t_0]\cos[2\omega t_0] - \sin[\omega t_0]\sin[2\omega t_0]\right)\right)t_t + \alpha\{t_0,\omega\}\frac{E_0}{\omega^2}\left(\varepsilon\sin[\omega t_0]\sin[2\omega t_0]\sinh[\omega t_t] + \frac{1}{4}\cos[\omega t_0]\cos[2\omega t_0]\sinh[2\omega t_t]\right) = 0 \tag{10}$$

Solving this equation yields the expression for $v_\perp$ that satisfies the abovementioned condition, encapsulating the complex interactions between the electron's momentum and the laser's electromagnetic field at the critical moment of ionization:

$$v_\perp\{\tau\} = \alpha\{t_0,\omega\}\frac{E_0}{\omega}\left[\varepsilon\left(\sin[\omega t_0]\sin[2\omega t_0] - \frac{1}{2}\cos[\omega t_0]\cos[2\omega t_0]\right) - \alpha\{t_0,\omega\}\frac{1}{\tau}\left(\varepsilon\sin[\omega t_0]\sin[2\omega t_0]\sinh[\tau] + \frac{1}{4}\cos[\omega t_0]\cos[2\omega t_0]\sinh[2\tau]\right)\right] \tag{11}$$

where $\tau = \omega t_t$, encapsulates the interaction duration relative to the cycle of the electromagnetic field. This variable serves as a bridge between the macroscopic parameters of the laser and the microscopic quantum dynamics of tunneling. Specifically, τ modulates how the temporal aspects of the laser's electromagnetic field influence the electron's transversal momentum during the critical moment of tunneling, providing a detail understanding of how field oscillations at the atomic level impact the electron's escape trajectory.

Building upon the dynamics captured by the variable τ, we advance our analysis by employing the saddle point equation to further elucidate the momentum components of the electron at the tunnel exit. The saddle point equation, crucial for identifying the conditions under which the electron's momentum components achieve optimal values, now can be defined by the expression: $[(p_x - E_0\sin[\omega(t_0+it_t)])/\omega) + \left(p_y - \varepsilon E_0\cos[2\omega(t_0+it_t)])/(2\omega)\right)]^2 + 2I_p = 0$. It is important to state that by using this foundational equation, we are able to derive explicit expressions for the momentum components at the tunnel exit. For the x−component:

$$p_x\{t_0,\tau\} = -\frac{E_0}{\omega}(2\varepsilon\delta\{t_0,\tau\}-1)\sin[\omega t_0]\cosh[\tau] \tag{12a}$$

and for the y − component:

$$p_y\{t_0,\tau\} = \frac{E_0}{\omega}\left(\delta\{t_0,\tau\} - \frac{\varepsilon}{2}\sin[\omega t_0]\cosh[2\tau]\right) \tag{12b}$$

where, $\delta\{t_0,\tau\}$ is introduced as a function defined by: $\delta\{t_0,\tau\} = \sqrt{\frac{\cos^2[\omega t_0]\sinh^2[\tau]-\gamma^2}{1+4\varepsilon^2\sin^2[\omega t_0]\cosh^2[\tau]}}$ (γ is the Keldysh parameter, defined as $\gamma = \sqrt{2I_p}/\omega$ [18]). This expression reflects the complex dependence of the electron's momentum components on the interplay between the field strength ratio of the laser field and the temporal dynamics encoded by τ. By resolving these momentum components, we gain a comprehensive understanding of how the electron's exit dynamics from the tunneling barrier are shaped not just by the instantaneous field values but also by the temporal evolution of the field across the tunneling event.

Having incorporated the refined momentum expressions from Eqs. (12) into Eq. (7), we can now derive the nonadiabatic instantaneous ionization rate:

$$W\{\omega,\tau\}\propto\exp\left[\left(\frac{E_0^2}{8\omega^2}\left(\varepsilon^2\cosh^2[2\tau]\sin^2[\omega t_0] - 4\varepsilon\delta\{t_0,\tau\}\cosh[2\tau]\sin[\omega t_0] + 4\left(\delta\{t_0,\tau\}^2 + (1-2\varepsilon\delta\{t_0,\tau\})^2\right)\cosh^2[\tau]\sin^2[\omega t_0]\right) + I_p + \frac{E_0^2}{4\omega^2}\left(1 + \frac{\varepsilon^2}{4}\right)\right)t_t + \frac{E_0^2\varepsilon^2}{64\omega^3}\sinh[4\tau]\cos[4\omega t_0] - \frac{E_0^2}{8\omega^3}\sinh[2\tau]\cos[2\omega t_0]\frac{E_0^2}{2\omega^3}\cosh[\tau]\sin^2[\omega t_0](-2+4\varepsilon\delta\{t_0,\tau\})\sinh[\tau] - \frac{\varepsilon E_0}{\omega}(\cosh[2\omega t_0]\sin[\omega t_0] + 2\delta\{t_0,\tau\})\sinh[2\tau]\right] \tag{13}$$

Our rate formula for an OTC laser field establishes the relation among key parameters such as field strength ratio, tunneling time, laser intensity, and angular frequency. This relationship is calculated along the most probable electron trajectory at a specific ionization time. The pre-exponential factor has been omitted for the sake of simplicity in the formulation.

Ionization dynamics in the presence of Coulomb potential

Building upon our foundational studies that explored ionization in the absence of Coulomb interactions, this subsection reintroduces the Coulomb potential to further refine our understanding of ionization dynamics. Traditional models like the SFA often neglect the long-range Coulomb forces exerted by the atomic nucleus [23,24,47], which can significantly enrich the understanding of electron dynamics under intense laser fields. Reintegrating the Coulomb potential into our models allows us to examine more realistic scenarios where the electrostatic force of the nucleus plays a crucial role. This force not only shapes the electron's trajectory, but also profoundly affects its ionization probability and energy states.

To quantitatively assess the impact of these forces, we should define the total ionization rate. his is accomplished by first determining the total imaginary part of the action, which combines the classical action (discussed in the previous section) and an additional term arising from the long-range Coulomb tail: $\mathrm{Im}\{S_t\} = \mathrm{Im}\{S\} + \mathrm{Im}\{S_c\}$. Accordingly, the total ionization rate can be expressed as the product of two components:

$$W_t\{v_\parallel, v_\perp, \tau\} = W\{v_\parallel, v_\perp, \tau\} \bullet W_c\{v_\parallel, v_\perp, \tau\} \tag{14}$$

Here, $W\{v_\parallel, v_\perp, \tau\}$ denotes the ionization rate previously derived in subsection 2.1 (see Eq. (13)) reflecting the direct interaction of the electron with the laser field, excluding Coulombic influences. Meanwhile, $W_c\{v_\parallel, v_\perp, \tau\}$ represents the additional contribution to the ionization rate from the Coulomb force exerted by the atomic nucleus. This term is calculated using the binding potential $V_b\{r_c(\tau)\} = -Z/|r_c(\tau)|$, where Z is the atomic number, and $r_c(\tau)$ denotes the classical trajectory of the electron as it moves through the Coulomb potential. This classical trajectory provides a path that the electron likely follows, influenced by both the external laser field and the electrostatic forces of the nucleus, offering a comprehensive view of the forces at play during ionization. In the present study, we define the total ionization rate by summing $W\{v_\parallel, v_\perp, \tau\}$ and $W_c\{v_\parallel, v_\perp, \tau\}$. This approach is based on the perturbative treatment framework, where the Coulomb correction is treated as a first-order perturbation to the ionization process. In such frameworks, perturbations are typically added as incremental adjustments to the zeroth-order term, particularly when their effects are small relative to the total action. This allows us to linearly superpose the effects of the Coulomb interaction on the ionization rate calculated without such interaction, consistent with linear response theory.

To precisely evaluate the total ionization rate, $W_t\{v_\parallel, v_\perp, \tau\}$, it is important to account for the Coulomb correction to the action (see Eq. (5)), which significantly influences the ionization process. This correction, denoted as $S_C\{r_c, \tau\}$, is crucial in understanding how the Coulomb potential shapes the electron's path through its ionization path. We calculate it by integrating the binding potential over the classical trajectory of the electron, expressed as:

$$S_C\{r_c,\tau\} = -\int_{t_s}^{t_0} V_b\{r_c(\tau)\}d\tau \tag{15}$$

Given the intense nature of the Coulomb force near the atomic nucleus, conventional perturbation methods fail to yield accurate results. Instead, we utilize a 'matching procedure' to evaluate this integral effectively as in [19,48]. This method involves splitting the integration process at an intermediate time, t_{im}, strategically chosen to closely align with the saddle time t_s. The integral is thus divided into two segments: $S_C(r_c,\tau) = -\int_{t_s}^{t_{im}} V_b\{r_c(\tau)\}d\tau - \int_{t_{im}}^{t_0} V_b\{r_c(\tau)\}d\tau$. The described approach becomes especially relevant in the sub-barrier region, where the electron's proximity to the nucleus enhances the Coulomb interaction's impact, markedly affecting the electron's potential energy and, consequently, its tunneling dynamics. By integrating the Coulomb force, we gain a comprehensive understanding of how these interactions modify the electron's trajectory and ionization rate under the full spectrum of the tunneling barrier.

To accurately simulate the ionization dynamics under the influence of both laser and Coulomb forces, an essential step is to compute the classical trajectory of the electron, $r_c(\tau)$, influenced predominantly by the laser's electromagnetic field. This trajectory calculation initiates from the classical equations of motion and under the OTC laser field (Eqs. (1) and (2)) can be expressed as:

$$r_c\{\tau,\varepsilon\} = -\frac{E_0}{\omega}\int_\tau^{t_s}\sin[\omega\tau]d\tau + \frac{\varepsilon E_0}{2\omega}\int_\tau^{t_s}\cos[2\omega\tau]d\tau \tag{16}$$

Upon performing the integrations and subsequent trigonometric trans-

formations, along with a Taylor expansion, we arrive at a refined expression for the trajectory:

$$r_c\{\tau,\varepsilon\} = \frac{E_0}{2}(\tau^2 - t_s^2)(1+\varepsilon) + \frac{\varepsilon E_0}{4\omega^2} \tag{17}$$

In Eq. (17), the electron trajectory $r_c\{\tau,\varepsilon\}$ is defined over the field strength ratio, ε [49]. When $\varepsilon = 0$, the trajectory corresponds to linear polarization, similar to the derivations found in Ref. [49]. The overall motion of the electron can be decomposed into two principal components based on the classically forbidden and allowed regions of motion. The forbidden part corresponds to the electron's motion under the potential barrier (quantum tunneling), and the allowed part corresponds to its free motion after emerging from under the barrier. This decomposition is mathematically represented by: $r_c\{\tau,\varepsilon\} = \mathrm{Im}\{r_c(\tau)\} + \mathrm{Re}\{r_c(\tau)\}$. To incorporate the effects of the barrier's quantum nature, we transform the saddle time t_s as $t_s \rightarrow ik/I_p$, where the parameter k is defined as: $k = \sqrt{2I_p}$ [50]. This simplifies the description of the electron's trajectory through the potential barrier as:

$$r_c\{\tau,\varepsilon\} = iE_0\frac{k}{I_p}(\tau - t_s)(1+\varepsilon) + \frac{\varepsilon E_0}{4\omega^2} \tag{18}$$

Here, the imaginary term, $\mathrm{Im}\{r_c(\tau)\}$, represents the sub-barrier component which describes the phase accumulated by the electron as it tunnels through the barrier. From a physical perspective, this is significant because it determines how the electron, under the influence of a field with varying field strength ratios, experiences and responds to the varying intensities of the electric field. This interaction plays an important role in determining the electron's tunneling probability, essentially dictating its chances of escaping the atomic potential despite classically insufficient energy to overcome it directly. Conversely, the real term, $\mathrm{Re}\{r_c(\tau)\}$, in Eq. (18), while generally minor in its effect, is not entirely negligible. It adjusts the trajectory by affecting the electron's interaction with the time-dependent oscillations of the electric field once it is outside the barrier. However, in numerous theoretical studies [7,28,51], primary focus is often placed on the imaginary component due to its dominant role in influencing the tunneling probability and dynamics under the barrier, with the real part providing supplementary adjustments to the electron's emergent behavior post-tunneling.

Having established the electron's trajectory using Eq. (18), we next focus on incorporating the Coulomb correction into our action calculations. To achieve this, as we have already stressed, one can employ the well-known method of introducing an intermediate time, t_{im}, as in Ref. [49]. This allows to segment the integration process of the Coulomb potential's influence over the trajectory, refining our analytical approach to:

$$S_C\{r_c,\tau\} = -\int_{t_s}^{t_{im}} V_b\{r_c(\tau)\}d\tau + \int_{im}^{t_0} V_b\{r_c(\tau)\}d\tau \tag{19}$$

To solve the first integral in Eq. (19), we apply a logarithmic transformation as in [28,49]. As a result, we get the following result: $-\int_{t_s}^{t_{im}} V_b\{r_c(\tau)\}d\tau = -i\frac{z}{k}\ln[kr_{im}]$, where r_{im} $ik(t_{im} - t_s)$ approximates the intermediate radial position in the Coulomb potential. For the second part of the integral, extending from the intermediate to the final time, we utilize exact solutions provided in the framework of the PPT theory [19] to obtain:

$$\int_{t_{im}}^{t_0} \frac{Z}{\mathrm{Im}\{r_c(\tau)\}}d\tau = i\frac{z}{k}\ln\left[\frac{t_s + t_{im}}{t_s - t_{im}}\right] \tag{20}$$

Integrating both solutions of the integrals presented in Eq. (19) gives us a complete expression for the Coulomb correction of the action, $\mathrm{Im}\{S_C\}$:

$$\mathrm{Im}\{S_C\} = -\frac{z}{k}\ln\left[\frac{2k^2}{(1+\varepsilon)E_0}\right] \tag{21}$$

This correction factor critically modifies the instantaneous ionization rate for the tunneling electron at time τ, which can now be expressed as:

$$W_t\{v\|, v_\perp, \tau\} \propto \exp[-2\mathrm{Im}\{S_t\}] \propto \left[\frac{(1+\varepsilon)E_0}{2k^2}\right]^{-\frac{2z}{k}} W\{v\|, v_\perp, \tau\} \tag{22}$$

Here, the Coulomb correction manifests as a multiplicative factor, $\left[\frac{(1+\varepsilon)E_0}{2k^2}\right]^{-\frac{2z}{k}}$, significantly impacting the rate depending on the electron's trajectory and the laser field's characteristics.

The Coulomb correction of the electron drift momentum

In laser-atom interactions, the Coulomb force from the atomic nucleus significantly affects the trajectory and behavior of an ionized electron. This section discusses how the Coulomb force alters the electron's drift momentum, which is essential for understanding the detailed motion of particles during strong-field ionization.

First, we introduce the total drift momentum, $p_t\{p_{tx}, p_{ty}, t_0\}$, as:

$$p_t\{p_{tx}, p_{ty}, t_0\} = \{p_x + p_{cx}\}\vec{e}_x + \{p_y + p_{cy}\}\vec{e}_y \tag{23}$$

where p_{cx} and p_{cy} are the Coulomb corrections to the momentum components along the x and y directions, respectively. These terms are determined by integrating the Coulomb force along the electron's path, influenced by the laser at the ionization time, t_0. Goreslavski's method [52] provides a practical way to calculate these corrections: $\vec{p}_c\{r_c, t_0\} = -\pi\sqrt{2r_c/E(t_0)}/4r_c^2(t_0) \times \vec{n}_{E(t_0)}$, where $\vec{n}_{E(t_0)} = \vec{E}(t_0)/\left|\vec{E}(t_0)\right|$ [53] is a unit vector aligned with the electric field at t_0: $\vec{n}_{E(t_0)} = \left[\cos[\omega t]\vec{e}_x + \varepsilon\sin[2\omega t]\vec{e}_y\right]/\sqrt{\cos^2[\omega t] + \varepsilon^2\sin^2[2\omega t]}$. These corrections are significant when the ionized electron has low initial velocities, as they strongly affect the electron's trajectory and its ultimate escape direction.

Integrating the effects of both the laser and Coulomb forces, the corrected components of the drift momentum are:

$$p_{tx}\{v\|, v_\perp\} = p_x\{v\|, v_\perp\} - \frac{\pi\sqrt{2r_c(t_0)/E(t_0)}}{4r_c^2(t_0)}\frac{E_0}{\sqrt{1+\varepsilon^2\tan(\omega t)^2}} \tag{24a}$$

$$p_{ty}\{v\|, v_\perp\} = p_y\{v\|, v_\perp\} - \frac{\pi\sqrt{2r_c(t_0)/E(t_0)}}{4r_c^2(t_0)}\frac{E_0\varepsilon\tan(\omega t)}{\sqrt{1+\varepsilon^2\tan(\omega t)^2}} \tag{24b}$$

These equations highlight the interaction between the Coulomb force and the laser field in shaping the electron's trajectory post-ionization. Grasping this interplay is essential for precisely depicting the electron's movement and the factors affecting its escape from the atomic potential.

Results and discussion

In this section, we investigate the TI of Ar atoms, frequently chosen for strong-field ionization studies due to their advantageous properties. With an ionization potential of $I_p = 15.76$ eV, Ar atoms provide consistent and well-documented ionization rates, making them ideal for studying fundamental ionization processes and validating theoretical models. Additionally, the relatively simple electronic structure of Ar allows for a reduction to a single active electron (SAE) model, simplifying the analysis without significant loss of accuracy. Our investigation focuses on ionization using OTC laser pulses, specifically at a wave-

length of 800 nm and peak intensities, I, ranging from 0.01 PWcm^{-2} to 1.00 PWcm^{-2}. These conditions are frequently employed in experimental setups (see [50]), providing relevance and practical applicability to our theoretical study. We have concentrated on single ionization events, which simplifies the complex multi-electron dynamics to a single active electron model [21]. This approach considers one electron explicitly while treating the remaining electrons as frozen. This simplification is justified by the dominance of single ionization processes under specific experimental conditions [31,51], thus enabling a more focused and computationally efficient analysis of the ionization mechanisms. Our analysis examines the impact of incorporating a Coulomb correction into the rate expression, specifically how it affects predictions made by Xie et al. [37]. We also compare these results with those derived from traditional ADK [20] and SFA [21] theories, offering a comprehensive evaluation of different theoretical frameworks. Additionally, we explore variations in the ionization rate as a function of the field strength ratio. This approach provides critical insights into the dynamics of *Ar* atoms subjected to strong-field conditions in two-dimensional (2D) laser fields. Through this comparative analysis, we aim to refine our understanding of how Coulomb corrections influence ionization rates, contrasting with and potentially enhancing the existing models. Understanding this impact is crucial for a comprehensive grasp of electron dynamics in complex laser fields, such as OTC. The findings from our study are compared with available experimental data and theoretical predictions from literature, specifically Refs. [20,21,52]. This comparison helps to validate our model and ensures consistency with established results. By systematically varying the field strength ratio and examining the resulting ionization rates, we aim to contribute to a deeper understanding of the fundamental processes that govern strong-field ionization in diverse laser field configurations.

Fig. 1 illustrates the temporal evolution of the instantaneous ionization rate for *Ar* atoms in an OTC field configuration, featuring two orthogonally polarized laser fields. This setup creates a complex environment for electron dynamics, highly sensitive to changes in the field strength ratio. The figure compares predictions from four theoretical models: the ADK model [20], the SFA model [21], the Xie et al. model [37], and the analytical nonadiabatic model introduced in this paper (see Eq. (22)). The analysis spans four different field strength ratios: $\varepsilon = 0.2$ (Fig. 1(a)), $\varepsilon = 0.4$ (Fig. 1(b)), $\varepsilon = 0.6$ (Fig. 1(c)), and $\varepsilon = 0.8$ (Fig. 1(d)). By examining these profiles, we can assess the impact of nonadiabatic effects and the initial momentum distribution on the ionization process. The selected range of field strength ratios allows for a systematic exploration of the effects from moderate to high field strength configurations while avoiding the complexities of near-maximum field strength conditions ($\varepsilon \to 1.0$). This specified range prevents the encounter with complex three-dimensional electron dynamics and significant magnetic field influences present when $\varepsilon \to 1.0$ [54], thereby maintaining the focus on the primary ionization mechanisms predominantly influenced by the varying components of the electric field within the laser interaction.

As the field strength ratio increases from $\varepsilon = 0.2$ (Fig. 1(a)) to $\varepsilon = 0.8$ (Fig. 1(d)), we observe a marked transition in the ionization profiles. The ionization rate at the lowest field strength ratio (Fig. 1(a)) is characterized by sharp, narrow peaks at critical phases of the laser's oscillating field. These peaks occur at critical times when the electric field's strength is maximized, correlating with the highest probability for efficient ionization. These conditions facilitate optimal electron tunneling through the potential barrier, as evidenced by the alignment of the electric field vector with the electron's potential escape trajectories. This efficiency is consistent across both the SFA and our nonadiabatic model, as observed in Fig. 1(a) and Fig. 1(b), where sharp peaks in ionization rates demonstrate optimal tunneling conditions. Conversely, the ADK model, based on assumptions of static fields [20], shows minimal variation across these field strength ratios, suggesting a less dynamic response to changes in field configuration. In contrast, the results of Xie et al. [37], with a broader distribution of ionization rates particularly

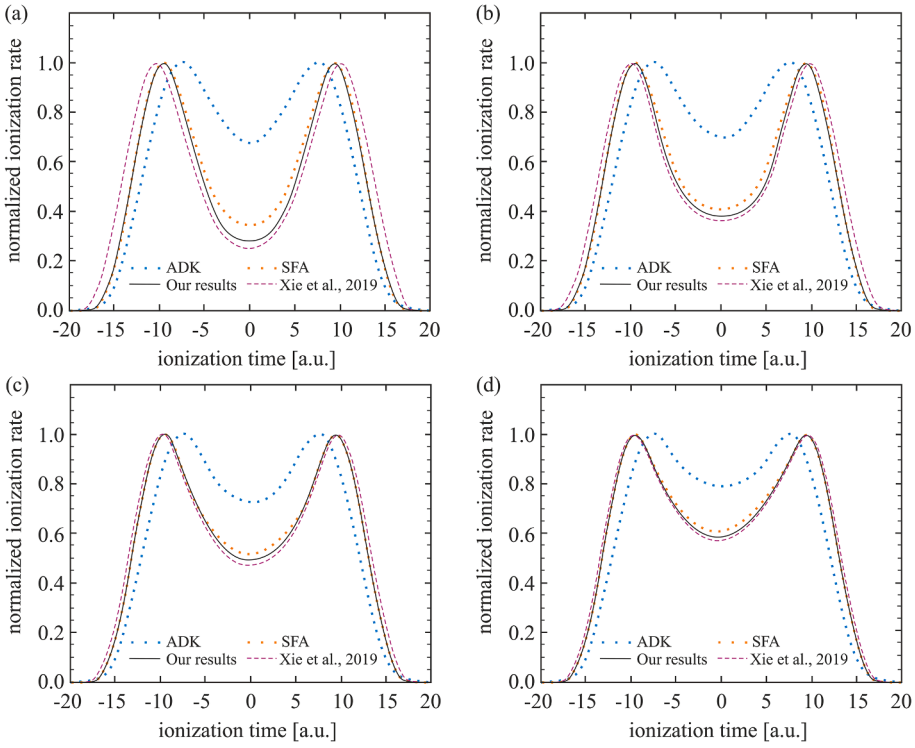

Fig. 1. The normalized ionization rate as a function of ionization time predicted by the ADK model (blue dashed line), the SFA model (orange dashed line), Xie et al. [37] model (purple dashed line) and the analytical nonadiabatic model (black line) in an OTC field (see Eq. (22)). The analysis is conducted for different field strength ratios: (a) $\varepsilon = 0.2$, (b) $\varepsilon = 0.4$, (c) $\varepsilon = 0.6$, and (d) $\varepsilon = 0.8$. (For interpretation of the references to color in this figure legend, the reader is referred to the web version of this article.)

noticeable at lower field strength ratios (Fig. 1(a) and Fig. 1(b)), highlight the importance of considering dynamic field effects. This broader distribution at lower ε values challenge traditional expectations and underscores the nuanced behavior of ionization dynamics [20,21]. Our model's closer alignment with the SFA [21] than Xie et al.'s results [37] can be attributed to how Coulomb corrections are treated in the tunneling process. While the SFA and our model consider dynamic changes in the electric field more comprehensively, Xie et al.'s model [37] may not fully account for the anisotropic effects of the Coulomb potential which become significantly impactful in scenarios with strong field alignments. In our approach, we incorporate these corrections to model how the Coulomb potential dynamically alters the potential barrier the electron experiences during tunneling. This includes adjustments based on the instantaneous position and velocity of the electron relative to the nucleus, which more accurately reflects the physical conditions under which ionization occurs. At higher field strength ratios, such as in Fig. 1(c) and Fig. 1(d), the field's polarization introduces additional perpendicular components. These components cause the electric field to oscillate in multiple directions, thus affecting the electron's path more drastically. These oscillations lead to variations in ionization times, which now extend around the peak electric field strength within each cycle. These components oscillate and significantly alter the electron's trajectory, leading to the observed variations in ionization times. Such variations extend both positively and negatively around the zero point on the ionization time scale, which represents the peak of the electric field strength within each cycle. The negative and positive ionization times reflect ionization events occurring before and after this peak, respectively, providing a comprehensive view of the electron dynamics throughout the electric field cycle. The dynamics at intermediate field strength ratios can be correlated with the results presented by [58], who noted that electron trajectories become significantly more chaotic as the field's polarization deviates from linear. This broadening of ionization peaks is indicative of the varying angles at which the electric field impacts ionization efficiency, reducing the probability of electrons aligning perfectly with the peak electric field strength. In Fig. 1(d), at a field strength ratio of $\varepsilon = 0.8$, the peaks broaden due to rapid shifts in the electric field's direction. This misalignment between the field vector and the electrons' optimal escape paths disrupts electron trajectories, thereby broadening the ionization peaks and reducing ionization efficiency. This behavior aligns with the theoretical predictions by [28,51]. In addition, as the field strength ratio increases, as observed in Fig. 1(c) and Fig. 1(d), noticeable discrepancies emerge between the models. Our analytical nonadiabatic model depicts a significant broadening and reduction in the amplitude of ionization peaks, a reflection of the dynamics induced by higher field strength ratios. This model's predictions underscore the impact of angular dispersion on the electric field vector, which misaligns the field with the electron's optimal tunneling trajectories, thus reducing ionization efficiency. In contrast, the ADK model continues to show relatively uniform profiles with only slight modulations, lacking the dynamic response observed in the other models. This uniformity at higher field strength ratios reveals the ADK model's fundamental inadequacy in capturing the complex, time-dependent behavior of electrons under non-linearly polarized fields. Overall, integrating Coulomb corrections into our model provides a more accurate representation of how electrons behave in strong laser fields, especially under conditions where $\varepsilon \to 1.0$. These corrections allow us to predict ionization rates more accurately and understand the complex behaviors of electrons, which are essential for advancing our understanding of atomic and molecular dynamics in high-intensity fields.

To deepen our understanding of ionization dynamics under varying field strength ratios, it is essential to examine both the temporal profiles and the spatial intensity distributions of the laser fields. Fig. 2 presents color maps of the laser intensity as a function of time, with the ionization rate represented by the color scale and provide a visual representation of the evolution of laser intensity over time and its impact on the ionization rate (see Eq. (22)).

At the lowest field strength ratio (see Fig. 2(a)), the intensity profile is characterized by symmetrical and sharp peaks. These peaks align with efficient ionization events as shown in Fig. 1(a), where the alignment of the electric field vector with the electron's potential escape direction is nearly optimal, facilitating effective tunneling through the potential barrier. The sharp peaks occur when the electric field is strongest and most effectively aligned, maximizing ionization probability. This happens because the orthogonal components of the laser fields combine to enhance the overall field strength at these points. This behavior is consistent with the one presented in Ref. [52]. As the field strength ratio increases, the profiles generally become broader but remain largely symmetrical as observed in Fig. 2(b) through 2(d). These profiles reflect the increased chaotic motion of electrons influenced by the orthogonal components of the electric field, as detailed in Fig. 1(b) and (c). The dashed lines are contour lines representing consistent ionization rates

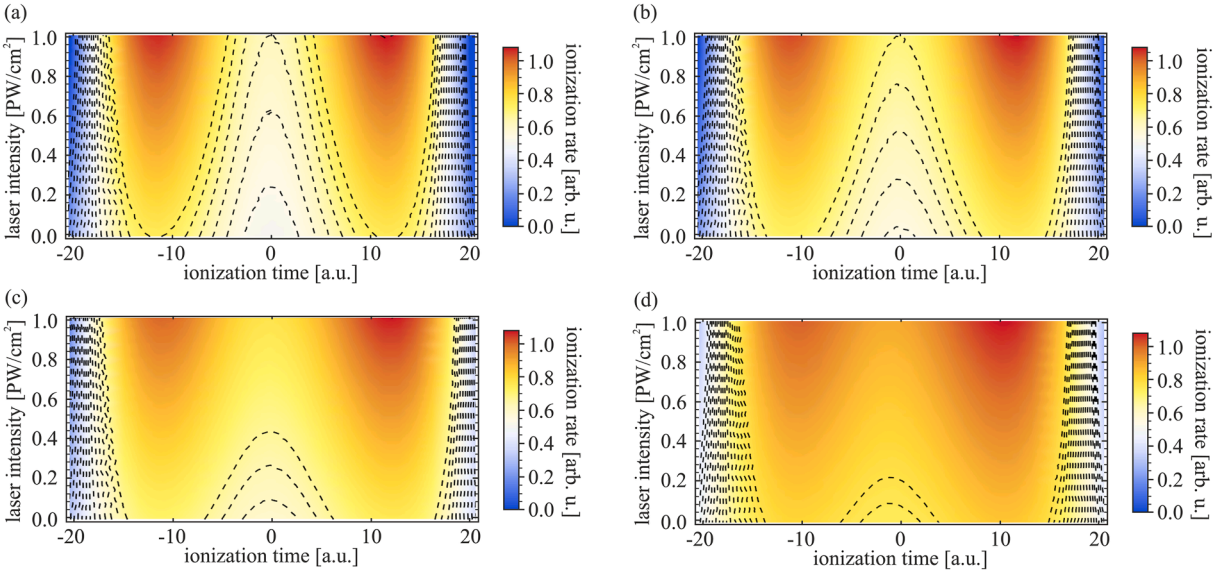

Fig. 2. Color maps of the laser intensity, I, as a function of ionization time, t, for different field strength ratios: (a) $\varepsilon = 0.2$, (b) $\varepsilon = 0.4$, (c) $\varepsilon = 0.6$, and (d) $\varepsilon = 0.8$. The color scale represents the ionization rate (in arb. u.).

across various ionization times and laser intensities, illustrating the dynamic phases of the oscillations and the interaction of the electric field with atomic electrons, thereby providing a clear view of how field geometry influences ionization dynamics. In Fig. 2(d), specifically at $\varepsilon = 0.8$, a slight asymmetry in the intensity profile is observed. This minor asymmetry results from the complex interplay of the two orthogonally polarized laser fields at high field strength ratios, where subtle nonadiabatic effects and the initial phase differences between the fields can induce discrepancies in electron motion. These conditions may not uniformly impact the ionization process across the oscillation cycle, leading to minor deviations from the expected symmetrical patterns. This asymmetry underscores the sensitivity of ionization dynamics to slight variations in field conditions, which can significantly affect the behavior of electrons under strong-field ionization. In Fig. 2(b), the broadening of the intensity profile signifies the onset of more field strength ratios. This broadening correlates with the increased chaotic motion of electrons as their trajectories become more sensitive to the perpendicular components of the electric field, as described in Fig. 1(b) and (c). Here, the field no longer provides a consistent direction for electron acceleration, leading to a spread in the kinetic energies and ejection angles of the ionized electrons. This complexity leads to greater variability in the ionization rates, which start to deviate from expected tunneling conditions. Observations from Fig. 2(c) reveal a broadening of the intensity profile and a noticeable decrease in peak intensities. These changes indicate a high field strength ratio, during which the rapid shifts in the electric field only occasionally align with the electron's most favorable escape trajectories. According to [59], this inconsistent alignment progressively decreases ionization efficiency, as electrons more frequently encounter suboptimal field orientations. In Fig. 2(d), the extensive expansion of the intensity profile, coupled with the lowest peak intensities, points to a very high field strength ratio. Under these conditions, the swift rotational dynamics of the field frequently cause a misalignment between the electric field and the electron's optimal tunneling paths, severely impacting the ionization dynamics. These findings highlight the complex interplay between field geometry, intensity, and Coulomb forces in shaping electron behavior in strong-field ionization, consistent with recent research reported in [51,55].

Following the detailed framework of our study, in Fig. 3 we present our findings on the effect of the field strength ratio on the cycle-averaged ionization rate of Ar atoms. The field strength ratio varies within the following range $0 < \varepsilon < 1$, while the rate is observed at two different laser intensities $I = 0.08\,\mathrm{PWcm^{-2}}$ (black solid line) and $I = 0.16\,\mathrm{PWcm^{-2}}$ (black dashed line).

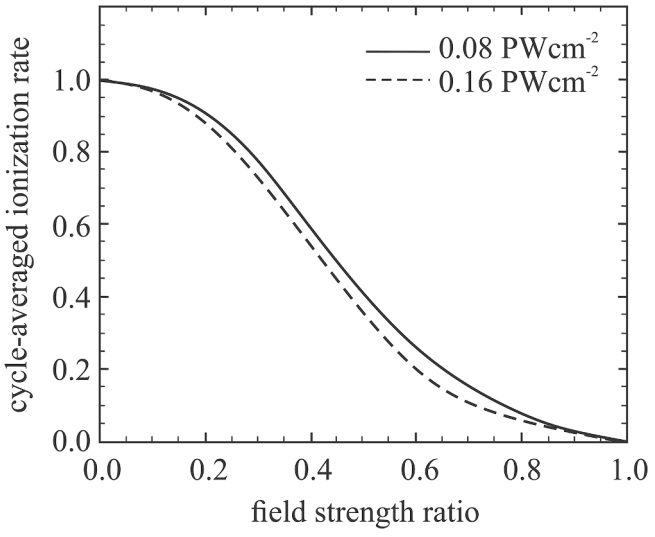

Fig. 3. Cycle-averaged ionization rate as a function of the field strength ratio at a central wavelength of 800 nm and peak intensities of $0.08\,\mathrm{PWcm^{-2}}$ and $0.16\,\mathrm{PWcm^{-2}}$.

As the field strength ratio increases, we observe a monotonous decline in the cycle-averaged ionization rate for both laser intensities. This decrease is more pronounced at the higher intensity of $0.16\,\mathrm{PWcm^{-2}}$, indicated by the steeper slope in the dashed line compared to the solid line for $0.08\,\mathrm{PWcm^{-2}}$. The observed trend is primarily influenced by the orientation and dynamic interaction of the laser's electric field components with the atomic system. According to [56,57], when the field strength of one component dominates, the electric field vector oscillates back and forth in a defined pattern, maximizing the electric field strength each cycle and providing a consistent directional force that can effectively dislodge an electron from its atomic orbit. As the field strength ratio increases, introducing a rotating field vector, the situation changes dramatically. The rotation spreads the vector's force over multiple directions within each cycle, thereby reducing the instantaneous field strength impacting the electron at any given moment. This decrease in effective field strength is critical because the ionization rate is highly dependent on the electron absorbing sufficient energy during its interaction with the field to overcome the ionization potential barrier. In field with maximum field strength ratio, the continuous rotation of the field vector dilutes this interaction, leading to a significant reduction in ionization rates as the field provides less directional energy transfer per cycle. From a theoretical perspective, the process can be understood through the Keldysh framework [18], which describes ionization in strong field regimes where the field's influence on electron motion is comparable to or dominates over the Coulomb potential of the nucleus. This framework indicates that as the field strength ratio increases, the ionization window – where the electron can absorb enough energy to escape – narrows significantly. Comparatively, OTC fields generate complex interference patterns that can periodically enhance the local field strength at certain field strength ratio settings, potentially increasing the ionization rate [57]. This is due to the unique superposition of two perpendicularly polarized laser fields which can constructively interfere, creating conditions momentarily similar to those in higher-intensity fields. In our analysis, discrepancies between ionization rates at different intensities underline the nonlinear dynamics of electron excitation and escape. At higher intensities, the field can induce more substantial distortion and stretching of the electron's wave packet, increasing the probability of ionization by providing multiple photon absorption pathways and enhancing the tunneling probability through increased field strength. Our findings emphasize the relationship between field geometry and electron dynamics, highlighting how varying field strength ratio can be used to control and manipulate ionization processes.

Building upon our comprehensive analysis of normalized ionization rates under variable field strength ratios, we now turn our focus to an examination of the electron drift momentum components, p_{tx} and p_{ty}, as outlined in Eqs. (24a) and (24b). The investigation of these momentum components is important; they encapsulate the cumulative effects of the laser's electric field and the characteristics of the electrons immediately post-ionization [51,55]. Fig. 4 presents a detailed comparative analysis of p_{tx} and p_{ty} across a range of laser intensities (from 0.01 $\mathrm{PWcm^{-2}}$ to 1.00 $\mathrm{PWcm^{-2}}$) and field strength ratios (from 0 to 1). Specifically, Figs. (a) and (c) explore these components at a fixed field strength ratio of $\varepsilon = 0.8$, providing a controlled context to assess the effects of varying intensities on these momentum dynamics. This analysis is aligned with theoretical models from Goreslavski et al. [52] and Dubois et al. [62], highlighted by blue and orange dashed lines, respectively. In Fig. 4(a), we delve into the dynamics of p_{tx} under these set conditions, critically assessing the accuracy of our models against these established theories. Similarly, Fig. 4(c) explores p_{ty}, offering insights into the transverse momentum dynamics influenced by the laser field at this specific field strength ratio. Further enriching this analysis, the color maps in Fig. 4(b) and 4(d) illustrate how p_{tx} and p_{ty} adapt to changes in both field strength ratio and laser intensity. These visualizations highlight the complex

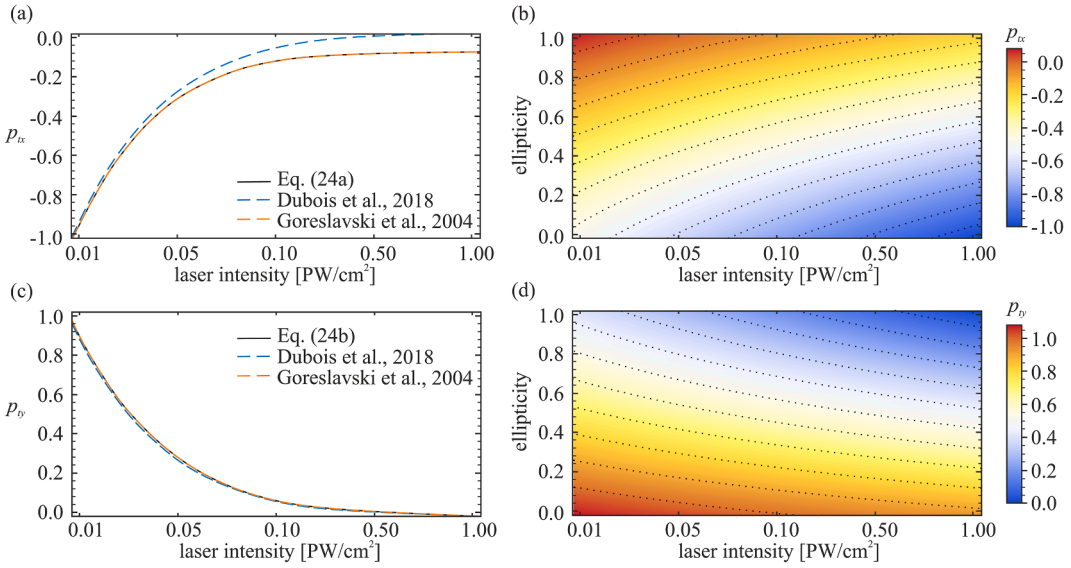

Fig. 4. The components p_{tx} and p_{ty} of the total drift momentum are explored under varying laser intensities, $0.01\,\mathrm{PWcm^{-2}} < I < 1.00\,\mathrm{PWcm^{-2}}$ and field strength ratio $0 < \varepsilon < 1$. In panel (a), p_{tx} is plotted and compared with the theoretical predictions from Goreslavski et al. [52] (orange dashed line) and Dubois et al. [60] (blue dashed line), while panel (c) presents a similar analysis for p_{ty}. Panels (b) and (d) further elucidate these relationships through color maps, which illustrate the dependency of p_{tx} and p_{ty} on I and ε, respectively.

interplay between the key parameters and provide a deeper understanding of the underlying mechanisms that govern electron dynamics in strong-field ionization within two-dimensional laser fields.

In Fig. 4(a) and 4(c), the drift momentum components p_{tx} and p_{ty} demonstrate distinct responses as laser intensity increases, observed within a fixed field strength ratio of $\varepsilon = 0.8$. This setting, approximating a high field strength ratio, offers a unique insight into the dynamics of electron drift momentum. From the results presented in Fig. 4(a), it is evident that at lower intensities ($I < 0.05\ PW/cm^2$), p_{tx} consistently exhibits a linear increase, reflecting efficient momentum transfer as the electric field's strength ideally aligns with the electron's initial trajectory. This behavior resonates well with the guiding-center model described by Dubois et al. [60], where electron dynamics in strong laser fields are modeled, particularly under conditions similar to high field strength ratios. The initial linear response also aligns with the asymmetrical effects on electron motion described by Goreslavski et al. [52], where the Coulomb force modifies trajectories during ionization, a phenomenon we observe as intensity increases. However, as the intensity surpasses $0.05\,\mathrm{PW/cm^2}$, notable deviations from Dubois's model [60] become evident. Our results, aligning more closely with Goreslavski et al. [52], suggest that our approach effectively captures the combined effects of non-linear ionization dynamics and the Coulomb potential's influence, aspects that are critical in high field strength ratio conditions but are less emphasized in Dubois's averaged models. This deviation highlights the significant role of the Coulomb potential in shaping electron trajectories, especially at higher intensities where the interaction becomes more pronounced, causing deviations from the predicted linear trajectory. This interaction becomes more distinct in fields with a high field strength ratio, where the initial drift momentum of the electron is considerable. This enables the Coulomb force to cause changes in the electron's path soon after ionization occurs. These changes are consistent with observations that the Coulomb potential, when combined with intense laser interactions, results in consistent asymmetries in electron motion, evident at all intensities [27]. In contrast, Fig. 4(c) presents a detailed analysis of p_{ty}, which displays a smooth and consistent decrease as laser intensity increases. This trend demonstrates the increasing influence of the perpendicular components of the electric field on the electron's motion. As intensity rises, these components progressively dominate the electron's dynamics, leading to a more pronounced influence on the electron's trajectory. These changes are primarily due to the increased impact of the field's oscillating components, which push and pull the electron in various directions, deviating from the more predictable paths observed at lower intensities. The excellent agreement with the theoretical assumptions of Dubois et al. [60] further corroborates that the models effectively capture these dynamics, highlighting the accurate simulation of the field's impact on electron behavior across varying intensities. The color maps in Fig. 4(b) and 4(d) further elaborate on these dynamics, illustrating how p_{tx} and p_{ty} adapt to a broader range of field strength ratios and intensities. In Fig. 4(d), rather than a broadening and diminution, the color gradient smoothly transitions with increasing intensity, reflecting a uniform adaptation of p_{ty} across the range of field strength ratios. This uniformity suggests a stable response of p_{ty} to changes in laser intensity and field strength ratio, contrary to a decrease in momentum efficiency. This behavior is indicative of the electron's ability to maintain a consistent momentum profile despite variations in field strength and polarization. Such a response underscores the nuanced interplay between field geometry and the electron's dynamics, rather than indicating a loss of momentum efficiency. The consistent color transition in Fig. 4(d) highlights how field strength ratio and intensity jointly influence the electron's trajectory, reflecting stability rather than the diminution of momentum under varied field conditions.

Conclusion

In this study, we have analyzed the ionization dynamics of Ar atoms in OTC laser fields. Incorporating the Coulomb potential into our model has allowed us to enhance our understanding of electron behavior across different field geometries, especially under strong laser conditions. We found that ionization rates decrease consistently as field strength ratio increases, highlighting the significant role of laser field geometry in influencing electron escape from atomic bonds. Notably, at higher field strength ratios, the distribution of the electric field's strength across orthogonal components leads to a reduction in the peak field experienced by the electron, thereby diminishing ionization efficiency. This study also shows that the ionization rate is increasingly sensitive to the temporal and spatial attributes of the laser field as intensity rises. This sensitivity results in broader ionization profiles at greater field strength

ratios, indicating complex electron dynamics influenced by the structured nature of OTC fields. These dynamics promote a range of electron behaviors, from optimal tunneling alignment to scenarios less conducive to ionization, emphasizing the critical impact of field geometry on ionization efficiency. Further, our analysis of drift momentum components reveals how electron behavior varies with changes in laser intensity at field strength ratios close to maximum balance. While electron behavior remains predictable at lower intensities, at higher intensities, we observe notable deviations. These deviations, characterized by increased angular dispersion and altered trajectories, largely result from the dynamic interactions between oscillating electric field components and the Coulomb potential. Overall, the presented study emphasizes the necessity of considering both the electric field and the Coulomb potential in ionization research and highlights the need for precise theoretical models that can capture these complex interactions. By delineating how these factors affect ionization under various conditions, we provide essential knowledge that is vital for enhancing control methods in laser-matter interaction experiments and applications.

Author statement

All authors have contributed equally to this manuscript.

CRediT authorship contribution statement

Hristina S. Delibašić-Marković: Writing – review & editing, Writing – original draft, Visualization, Validation, Supervision, Software, Resources, Project administration, Methodology, Investigation, Funding acquisition, Formal analysis, Data curation, Conceptualization. **Violeta M. Petrović:** Conceptualization, Data curation, Formal analysis, Funding acquisition, Investigation, Methodology, Project administration, Resources, Software, Supervision, Validation, Visualization, Writing – original draft, Writing – review & editing. **Ivan D. Petrović:** Conceptualization, Data curation, Formal analysis, Funding acquisition, Investigation, Methodology, Project administration, Resources, Software, Supervision, Validation, Visualization, Writing – original draft, Writing – review & editing.

Declaration of competing interest

The authors declare that they have no known competing financial interests or personal relationships that could have appeared to influence the work reported in this paper.

Acknowledgements

Authors would like to acknowledge the support received from the Science Fund of the Republic of Serbia, #GRANT 6821, Atoms and (bio) molecules-dynamics and collisional processes on short time scale - ATMOLCOL. Our appreciation also goes to the Serbian Ministry of Education, Science and Technological Development (Agreement No. 451-03-66/2024-03/ 200122). H. Delibasic Markovic would also like to express gratitude to COST Actions CA21159 - “Understanding interaction of light with biological surfaces: possibility for new electronic materials and devices (PhoBioS)” for their support and CA22148 - “An international network for Non-linear Extreme Ultraviolet to hard X-ray techniques (NEXT)”.

Data availability

No data was used for the research described in the article.

References

[1] Schleif T, Prado Merini M, Henkel S, Sander W. Solvation effects on quantum tunneling reactions. Acc Chem Res 2022;55:2180–90. https://doi.org/10.1021/acs.accounts.2c00151.
[2] Tan J, Xu S, Han X, Zhou Y, Li M, Cao W, et al. Resolving and weighing the quantum orbits in strong-field tunneling ionization. Adv Photonics 2021;3:035001–6. https://doi.org/10.1117/1.AP.3.3.035001.
[3] Sainadh US, Sang RT, Litvinyuk IV. Attoclock and the quest for tunnelling time in strong-field physics. J Phys Photonics 2020;2:042002. https://doi.org/10.1088/2515-7647/aba009.
[4] Nader DJ, González-Rodríguez CA, Lerma-Hernández S. Avoided crossings and dynamical tunneling close to excited-state quantum phase transitions. PhysRevE 2021;104:064116. https://doi.org/10.1103/PhysRevE.104.064116.
[5] Kaleris K, Kaniolakis-Kaloudis E, Aravantinos-Zafiris N, Katerelos DT, Dimitriou VM, Bakarezos M, et al. Acoustic metamaterials characterization via laser plasma sound sources. Commun Mater 2024;5:93. https://doi.org/10.1038/s43246-024-00529-w.
[6] Cui J, Yang B, Luo X, Li L, Yu X. Controlling light tunneling by adiabatic passage in two modulated nonlinear waveguides. Results Phys 2019;15:102792. https://doi.org/10.1016/j.rinp.2019.102792.
[7] Petrović VM, Marković HSD, Petrović ID. Ionization rate in an elliptically polarized laser field with respect to momentum at the tunneling exit point for noble atoms. Results Phys 2023;53:107005. https://doi.org/10.1016/j.rinp.2023.107005.
[8] Peters O, Bogdanoff N, Acero González S, Melischek L, Simon JR, Reecht G, et al. Resonant Andreev reflections probed by photon-assisted tunnelling at the atomic scale. Nat Phys 2020;16:1222–6. https://doi.org/10.1038/s41567-020-0972-z.
[9] Wu D, Guo FM, Wang J, Chen JG, Yang YJ. Precollision effect on the double ionization of an Ar atom driven by a two-color counter-rotating circularly polarized laser pulse. Results Phys 2023;54:107123. https://doi.org/10.1016/j.rinp.2023.107123.
[10] Liu F, Li S, Chen Z, Böning B, Fritzsche S. Nonsequential double ionization of Ne with elliptically polarized laser pulses. PhysRevA 2022;106:043120. https://doi.org/10.1103/PhysRevA.106.043120.
[11] Yan JZ, Zhao SS, Lan WD, Li SY, Zhou SS, Chen JG, et al. Calculation of high-order harmonic generation of atoms and molecules by combining time series prediction and neural networks. Opt Express 2022;30:35444–56. https://doi.org/10.1364/OE.470495.
[12] Schneider L, Beck P, Wiebe J, Wiesendanger R. Atomic-scale spin-polarization maps using functionalized superconducting probes. Sci Adv 2021;7:eabd7302. https://doi.org/10.1126/sciadv.abd7302.
[13] Xie W, Yan J, Li M, Cao C, Guo K, Zhou Y, et al. Picometer-resolved photoemission position within the molecule by strong-field photoelectron holography. PhysRevLett 2021;127:263202. https://doi.org/10.1103/PhysRevLett.127.263202.
[14] Yang J, Zhu X, Nunes JPF, Yu JK, Parrish RM, Wolf TJ, et al. Simultaneous observation of nuclear and electronic dynamics by ultrafast electron diffraction. Science 2020;368:885–9. https://doi.org/10.1126/science.abb2235.
[15] Heldt T, Dubois J, Birk P, Borisova GD, Lando GM, Ott C, et al. Attosecond real-time observation of recolliding electron trajectories in helium at low laser intensities. PhysRevLett 2023;130:183201. https://doi.org/10.1103/PhysRevLett.130.183201.
[16] Kaleris K, Orphanos Y, Bakarezos M, Papadogiannis N, Mourjopoulos J. The effect of geometry on the acoustic radiation of plasma filaments in air. Forum Acusticum 2020:1819–26. https://doi.org/10.48465/fa.2020.1013.
[17] Ganeev RA, Mirzaev BS. Atomic versus molecular plasmas for frequency conversion of laser radiation: stronger harmonics, larger cutoffs, better stability, resonance, and quasi-phase-matching enhancement. Appl Phys B 2024;130:1–10. https://doi.org/10.1007/s00340-024-08216-x.
[18] Keldysh LV. Ionization in the field of a strong electromagnetic wave. Sov Phys JETP 1965;20:1307. https://doi.org/10.1142/9789811279461_0008.
[19] Perelomov AM, Popov VS, Terent'ev MV. Ionization of atoms in an alternating electric field. Sov Phys JETP 1966;23:924–34.
[20] Ammosov MV, Delone NB, Krainov VP. Tunnel ionization of complex atoms and of atomic ions in an alternating electromagnetic field. Sov Phys JETP 1986;64:1191.
[21] Salières P, Carré B, Le Déroff L, Grasbon F, Paulus GG, Walther H, et al. Feynman's path-integral approach for intense-laser-atom interactions. Science 2001;292:902–5. https://doi.org/10.1126/science.108836.
[22] Ivanov IA, Kim KT. Distribution of absorbed photons in the tunneling ionization process. Sci Rep 2021;11:3956. https://doi.org/10.1038/s41598-021-83453-0.
[23] Faisal FHM. Strong-field S-matrix theory with final-state Coulomb interaction in all orders. PhysRevA 2016;94:031401. https://doi.org/10.1103/PhysRevA.94.031401.
[24] Reiss HR. Energetic electrons in strong-field ionization. PhysRevA 1996;54:R1765. https://doi.org/10.1103/PhysRevA.54.R1765.
[25] Becker A, Faisal FH. Correlated Keldysh-Faisal-Reiss theory of above-threshold double ionization of He in intense laser fields. PhysRevA 1994;50:3256. https://doi.org/10.1103/PhysRevA.50.3256.
[26] Becker W, Lohr A, Kleber M. Light at the end of the tunnel: two-and three-step models in intense-field laser-atom physics. Quantum Semiclass Opt 1995;7:423. https://doi.org/10.1088/1355-5111/7/3/017.
[27] Becker W, Liu X, Ho PJ, Eberly JH. Theories of photoelectron correlation in laser-driven multiple atomic ionization. RevModPhys 2012;84:1011–43. https://doi.org/10.1103/RevModPhys.84.1011.
[28] Petrović V, Marković HD, Petrović I. Coulomb corrected nonadiabatic instantaneous ionization rate and the electron trajectory in an elliptically polarized

laser field. Results Phys 2023;51:106718. https://doi.org/10.1016/j.rinp.2023.106718.
[29] Bai Y, Hao X, Li W, Yang W, Chen J. Coulomb-corrected quantum-trajectories method for recollision-impact double ionization in an intense laser field. PhysRevA 2023;108:013115. https://doi.org/10.1103/PhysRevA.108.013115.
[30] Ren D, Chen C, Li X, Zhao X, Wang S, Li M, et al. Transverse momentum resolved angular streaking after tunneling ionization. PhysRevRese 2023;5:L032044. https://doi.org/10.1103/PhysRevResearch.5.L032044.
[31] Huang C, Zhong M, Wu Z. Nonsequential double ionization by co-rotating two-color circularly polarized laser fields. Opt Express 2019;27:7616–26. https://doi.org/10.1364/OE.27.007616.
[32] Zhao Y, Zhou Y, Liang J, Zeng Z, Ke Q, Liu Y, et al. Frustrated tunneling ionization in the elliptically polarized strong laser fields. Opt Express 2019;27:21689–700. https://doi.org/10.1364/OE.27.021689.
[33] Geyer A, Trabert D, Hofmann M, Anders N, Schöffler MS, Schmidt LPH, et al. Experimental fingerprint of the electron's longitudinal momentum at the tunnel exit in strong field ionization. PhysRevRese 2023;5:033094. https://doi.org/10.1103/PhysRevResearch.5.033094.
[34] Zhang S, Zhang G, Liu K, Shi W, Yao J. Numerical investigation on Coulomb impact on bouquetlike photoelectron momentum distributions. J Mod Opt 2023;70:564–71. https://doi.org/10.1080/09500340.2023.2294437.
[35] Feng Y, Li M, Luo S, Liu K, Du B, Zhou Y, et al. Semiclassical analysis of photoelectron interference in a synthesized two-color laser pulse. PhysRevA 2019;100:063411. https://doi.org/10.1103/PhysRevA.100.063411.
[36] Cheng H, Liu S, Li P, Liu F, Han L, Qi S, et al. Femtosecond laser-induced spatial-frequency-shifted nanostructures by polarization ellipticity modulation. Opt Express 2021;29:29766–79. https://doi.org/10.1364/OE.434363.
[37] Xie W, Li M, Luo S, He M, Liu K, Zhang Q, et al. Nonadiabaticity-induced ionization time shift in strong-field tunneling ionization. PhysRevA 2019;100:023414. https://doi.org/10.1103/PhysRevA.100.023414.
[38] Xie X, Chen C, Xin G, Liu J, Chen Y. Coulomb-induced ionization time lag after electrons tunnel out of a barrier. Opt Express 2020;28:33228–39. https://doi.org/10.1364/OE.408424.
[39] Agueny H. Quantum control and characterization of ultrafast ionization with orthogonal two-color laser pulses. Sci Rep 2020;10:239. https://doi.org/10.1038/s41598-019-57125-z.
[40] Milošević DB. Quantum theory of photon emission during strong-laser-field-induced ionization. PhysRevA 2023;108:033110. https://doi.org/10.1103/PhysRevA.108.033110.
[41] Gao F, Chen YJ, Xin GG, Liu J, Fu LB. Distilling two-center-interference information during tunneling of aligned molecules with orthogonally polarized two-color laser fields. PhysRevA 2017;96:063414. https://doi.org/10.1103/PhysRevA.96.063414.
[42] Ludwig A, Maurer J, Mayer BW, Phillips CR, Gallmann L, Keller U. Breakdown of the dipole approximation in strong-field ionization. PhysRevLett 2014;113:243001. https://doi.org/10.1103/PhysRevLett.113.243001.
[43] Liu MM, Liu Y. Semiclassical models for strong-field tunneling ionization of molecules. J Phys b: at Mol Opt Phys 2017;50:105602. https://doi.org/10.1088/1361-6455/aa6a3e.
[44] Chen Z, Morishita T, Le AT, Wickenhauser M, Tong XM, Lin CD. Analysis of two-dimensional photoelectron momentum spectra and the effect of the long-range Coulomb potential in single ionization of atoms by intense lasers. PhysRevA 2006;74:053405. https://doi.org/10.1103/PhysRevA.74.053405.
[45] Yudin GL, Ivanov MY. Physics of correlated double ionization of atoms in intense laser fields: quasistatic tunneling limit. PhysRevA 2001;63:033404. https://doi.org/10.1103/PhysRevA.63.033404.
[46] Li M, Geng JW, Han M, Liu MM, Peng LY, Gong Q, et al. Subcycle nonadiabatic strong-field tunneling ionization. PhysRevA 2016;93:013402. https://doi.org/10.1103/PhysRevA.93.013402.
[47] Keil T, Bauer D. Coulomb-corrected strong-field quantum trajectories beyond dipole approximation. J Phys B: At Mol Opt Phys 2017;50:194002. https://doi.org/10.1088/1361-6455/aa8ab1.
[48] Kaushal J, Smirnova O. Nonadiabatic Coulomb effects in strong-field ionization in circularly polarized laser fields. PhysRevA 2013;88:013421. https://doi.org/10.1103/PhysRevA.88.013421.
[49] Long Z. Theoretical Study of Non-Relativistic Electron Dynamics Under Intense Laser Fields. University of Waterloo; 2012. Doctoral dissertation.
[50] Li M, Liu MM, Geng JW, Han M, Sun X, Shao Y, et al. Experimental verification of the nonadiabatic effect in strong-field ionization with elliptical polarization. PhysRevA 2017;95:053425. https://doi.org/10.1103/PhysRevA.95.053425.
[51] Luo S, Li M, Xie W, Liu K, Feng Y, Du B, et al. Exit momentum and instantaneous ionization rate of nonadiabatic tunneling ionization in elliptically polarized laser fields. PhysRevA 2019;99:053422. https://doi.org/10.1103/PhysRevA.99.053422.
[52] Goreslavski SP, Paulus GG, Popruzhenko SV, Shvetsov-Shilovski NI. Coulomb asymmetry in above-threshold ionization. PhysRevLett 2004;93:233002. https://doi.org/10.1103/PhysRevLett.93.233002.
[53] Dura J, Camus N, Thai A, Britz A, Hemmer M, Baudisch M, et al. Ionization with low-frequency fields in the tunneling regime. Sci Rep 2013;3:2675. https://doi.org/10.1038/srep02675.
[54] Hartung A, Eckart S, Brennecke S, Rist J, Trabert D, Fehre K, et al. Magnetic fields alter strong-field ionization. Nat Phys 2019;15:1222–6. https://doi.org/10.1038/s41567-019-0653-y.
[55] Chen C, Ji XX, Li WY, Han X, Chen YJ. Local most-probable routes and classical-quantum correspondence in strong-field two-dimensional tunneling ionization. PhysRevA 2021;104:013106. https://doi.org/10.1103/PhysRevA.104.013106.
[56] Liu K, Luo S, Li M, Li Y, Feng Y, Du B, et al. Detecting and characterizing the nonadiabaticity of laser-induced quantum tunneling. PhysRevLett 2019;122:053202. https://doi.org/10.1103/PhysRevLett.122.053202.
[57] Xie X, Wang T, Yu S, Lai X, Roither S, Kartashov D, et al. Disentangling intracycle interferences in photoelectron momentum distributions using orthogonal two-color laser fields. PhysRevLett 2017;119:243201. https://doi.org/10.1103/PhysRevLett.119.243201.
[58] Ying L, Wang G, Huang L, Lai YC. Quantum chaotic tunneling in graphene systems with electron-electron interactions. PhysRevB 2014;90:224301. https://doi.org/10.1103/PhysRevB.90.224301.
[59] Milošević DB. Application of quantum-orbit theory to atomic processes in strong tailored laser fields and terahertz pulses. Eur Phys J plus 2023;138:356. https://doi.org/10.1140/epjp/s13360-023-03962-x.
[60] Dubois J, Berman SA, Chandre C, Uzer T. Capturing Photoelectron Motion with Guiding Centers. PhysRevLett 2018;121:113202. https://doi.org/10.1103/PhysRevLett.121.113202.